Proceedings of the 2012 20th International Conference on Nuclear Engineering
collocated with the
ASME 2012 Power Conference
ICONE20-POWER2012
July 30 - August 3, 2012, Anaheim, California, USA

ICONE20-POWER2012-54320

STABILITY ANALYSIS FOR REACTOR COOLANT PUMP WITH VERTICAL ROTOR SUPPORTED BY FLUID FILM BEARINGS

Yaoyu HU
Shanghai Jiao Tong University
Shanghai, China

Dezhong WANG
Shanghai Jiao Tong University
Shanghai, China

Yujin WANG
Shanghai Jiao Tong University
Shanghai, China

Jige ZHANG
Shanghai Jiao Tong University
Shanghai, China

Weiguo GU
Shanghai Jiao Tong University
Shanghai, China

ABSTRACT

A special dynamics model for a vertical rotor-bearing system with two fly wheels is developed, imitating a sort of reactor coolant pump (RCP) under design. The stability and the process of reaching that condition are of special interest since the rotor is supported vertically other than horizontally. And the classical Jeffcott rotor dynamics model is not quite appropriate because the real pump has its two fly wheels outside the region between the two journal bearings and it has a thrust bearing right under the lower fly wheel. A set of dynamics coefficients are introduced to the rotor dynamics model, taking account of the flow confinement in the reduced gap of the canned pump. The stability characteristic is clearly changed due to the additional dynamics coefficients. Numerical simulation shows that the critical speed of the RCP is lowered. The moment of the thrust bearing, which is ignored customarily in rotor dynamics analysis, also influences the dynamic behavior of the rotor system. The stability of the rotor is enhanced while the thrust bearing has its stiffness and damping values in certain ranges.

Key words: RCP, stability analysis, thrust bearing

INTRODUCTION

Reactor coolant pump (RCP) is the only component under continuous operation, known as the 'heart' of the primary coolant loop (or RCS, Reactor Coolant System) of a standard pressurized water reactor. The stability of RCP is of great importance for it has the same lifetime of the reactor, which is 60 years, and zero maintenance requirements during its entire service time, according to the newly designed reactor system deployed in China. Rotor dynamics of RCP is the central part of its stability characteristics. The RCP configuration under design is a vertical centrifugal water pump equipped with a canned motor, two fly wheels, two journal bearings and a thrust bearing. The annular flow due to the fluid confinement between the rotor and stator of the canned motor together with the thrust bearing can bring considerable influences to the rotor dynamics stability characteristics of the RCP.

The canned motor of RCP will produce a fluid-structure interaction feature from the annular flow in the reduced gap, which has significantly different dimension and flow characteristic from bearings and seals, between the rotor and stator. Some prior works are done by Fritz [1] and Ramsden *et al.* [2, 3]. Antunes, Grunenwald and Moreira *et al.* [4, 5, 6] have done a series of theoretical and experimental researches on the vibration of rotating shafts subjected to this kind of fluid-structure interaction. Antunes *et al.* investigated the steady and fluctuating flow in the reduced gap theoretically with concentric and eccentric configurations [4] and explored the influences of the dissipative effects from the friction of the fluid boundaries [6]. Antunes *et al.* described the added mass and coupled dynamics coefficients, namely the inertial coupling coefficients, damping and stiffness coefficients, as functions of eccentricity ε, rotor angular velocity Ω, and rotor dimension parameters. Their work shows that the stability of the rotor bearing system has been changed greatly with the existence of the annular flow. As the RCP has the concentric configuration, which indicates ε=0 (dimensionless eccentricity), the stability analysis should exhibits similar results with that done by Antunes *et al.*, in concentric situation.

Lots of efforts have been done on the lateral vibration of a shaft supported by fluid film journal bearings. In contrast, the

influence of thrust bearings gains much less attention. However, the support of RCP under research has two journal bearings and one double direction thrust bearing, and the latest experiments show that the thrust bearing does indeed play a vital part in the stability characteristics of the whole rotor bearing system. Consequently, certain stability analysis, with the thrust bearing in consideration, must be done. Previous work shows cases that thrust bearing greatly changes the dynamic characteristics of rotor bearing systems [7]. Mittwollen *et al.* [8] studied the effect of thrust bearing on the dynamics of a single-mass rotor system. Jiang *et al.* [9, 10] thoroughly studied this issue theoretically and have done some numerical simulation about thrust bearing, giving out the coupled dynamics coefficients. Jiang *et al.* [9] also discussed some potential factors that will influence the effect of thrust bearing on a rotor bearing system. Since the RCP places the two fly wheels outside the region between the two journal bearings, instead of the Jeffcott-like model that found in previously mentioned works, a special model is needed.

A detailed finite element model has been built, considering the fluid structure interaction of the RCP motor and the effect comes with the thrust bearing at the very bottom of the lower fly wheel. The numerical computation reveals that the critical speed of the rotor bearing system is clearly changed. The stability characteristic is investigated in a wide range of dynamics coefficients of the thrust bearing, arriving at several stability charts, and the results make it clear that some whirl motions become unstable when the system is operating in certain speed range.

MODEL AND FORMULATION

Basic finite element model of the RCP

Configuration of the rotor bearing system of the interested RCP is settled down in recent years, which is a vertical rotor pump with its impeller at the top. As shown in Fig. 1, the rotor is supported on two journal bearings and a double direction thrust bearing. There is a canned motor between the two journal bearings. This RCP conveys coolant, almost water, in the primary loop of the RCS. All the three bearings take the water of the RCS as their lubricant. From the draft in Fig. 1, a path of water flow, including the water that lubricating the bearings and that in the reduced gap of the motor, can be found (The actual flow direction and route may not be the same as Fig. 1. But it does not affect the present analysis.).

A finite element model, with 23 elements and 24 nodes, is depicted in Fig. 2. The detailed dimensions are around the actual dimension values. The two fly wheels and the impeller are simplified as three rigid disks and attached to Node 3, 21 and 24, respectively. Node 6 and 19 are the places where the journal bearings are. The thrust bearing is settled at Node 5. As shown in Fig. 2, in the specified coordinate, two displacement variables are defined as Eq. (1).

$$\{u_{1,j}\}=\begin{Bmatrix} x_j \\ \theta_{yj} \end{Bmatrix}, \{u_{2,j}\}=\begin{Bmatrix} y_j \\ -\theta_{xj} \end{Bmatrix} \tag{1}$$

where θ_x and θ_y are the angular displacements along x-axis and y-axis. The assembled system equation is Eq. (2), in the usual form of common dynamics problem

$$\left.\begin{aligned} [M_1]\{\ddot{U}_1\}+\Omega[J_1]\{\dot{U}_2\}+[K_1]\{U_1\}=\{Q_1\} \\ [M_1]\{\ddot{U}_2\}-\Omega[J_1]\{\dot{U}_1\}+[K_1]\{U_2\}=\{Q_2\} \end{aligned}\right\} \tag{2}$$

where $[M_1]$, $\Omega[J_1]$ and $[K_1]$ are the assembled system inertia, gyroscopic and stiffness matrices, with Ω represents the angular speed. All the three coefficient matrices are symmetric and derived from Timoshenko beam theory. The displacement vectors for the system are

$$\left.\begin{aligned} \{U_1\} &= [u_{1,1}, u_{1,2}, \cdots, u_{1,24}]^T \\ &= [x_1, \theta_{y1}, x_2, \theta_{y2}, \cdots, x_{24}, \theta_{y24}]^T \\ \{U_2\} &= [u_{2,1}, u_{2,2}, \cdots, u_{2,24}]^T \\ &= [y_1, -\theta_{x1}, y_2, -\theta_{x2}, \cdots, y_{24}, \theta_{x24}]^T \end{aligned}\right\} \tag{3}$$

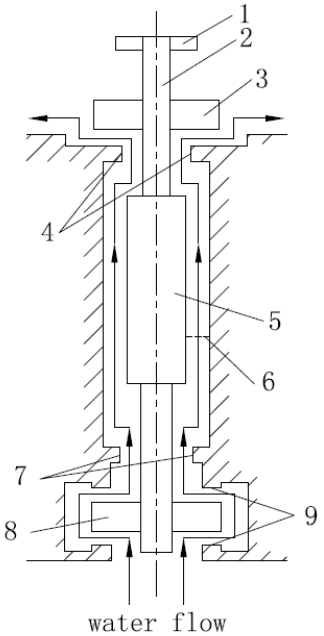

Fig. 1. Configuration of the RCP.
1-impeller disk; 2-shaft(or rotor); 3-upper fly wheel; 4-upper journal bearing; 5-rotor of canned motor; 6-reduced gap of canned motor; 7-lower journal bearing; 8-lower fly wheel; 9-double side thrust bearing.

where the footnote of x_j denotes the jth node of the finite element model. $\{Q_1\}$ and $\{Q_2\}$ in Eq. (2) are generic forces that include the effects of mass unbalance and other external forces.

The impeller of the RCP is simplified into a rigid disk. The three disks put additional coefficients at the diagonal of $[M_1]$ and $[J_1]$. Table 1 shows the coefficients of the disks (or fly wheels) used in the stability analysis.

The final dynamics equation of the rotor can be derived naturally from Eq. (2). That is

$$[M_r]\{\ddot{U}\}+[C_r]\{\dot{U}\}+[K_r]\{U\}=\{Q\} \tag{4}$$

where

$$[M_r]=\begin{bmatrix} M_1 & \\ & M_1 \end{bmatrix},[C_r]=\begin{bmatrix} c_{11} & c_{12}+\Omega J_1 \\ c_{21}-\Omega J_1 & c_{22} \end{bmatrix},$$

$$[K_r]=\begin{bmatrix} k_{11}+K_1 & k_{12} \\ k_{21} & k_{22}+K_1 \end{bmatrix},$$

$$\{U\}=\begin{Bmatrix} U_1 \\ U_2 \end{Bmatrix},\{Q\}=\begin{Bmatrix} Q_1 \\ Q_2 \end{Bmatrix} \tag{5}$$

In Eq. (5), the matrices [k_{ij}] and [c_{ij}] (i=1, 2, j=1, 2) are the coefficient matrices of journal bearings. These bearing coefficient values used in the stability analysis are in good agreement with the actual pump.

Table 1 Coefficients of disks.

Node No.	*Mass (kg)*	*section inertia (kg m^4)*	*polar moment of inertia (kg m^4)*
3	3000	250	400
21	3000	250	400
24	500	20	40

Fluid confinement of the annular flow

For the interested RCP, the dimension of the reduced gap between the rotor and stator can be chosen as 5mm. The force on one node of an element due to fluid-structure interaction can be described as Eq. (6) according to the theoretical results of Antunes' work [4].

$$\begin{Bmatrix} F^e_{fs,x} \\ F^e_{fs,y} \end{Bmatrix}=-\begin{bmatrix} m^e_{xx} & m^e_{xy} \\ m^e_{yx} & m^e_{yy} \end{bmatrix}\begin{Bmatrix} \ddot{x} \\ \ddot{y} \end{Bmatrix}-\begin{bmatrix} c^e_{xx} & c^e_{xy} \\ c^e_{yx} & c^e_{yy} \end{bmatrix}\begin{Bmatrix} \dot{x} \\ \dot{y} \end{Bmatrix}-\begin{bmatrix} k^e_{xx} & k^e_{xy} \\ k^e_{yx} & k^e_{yy} \end{bmatrix}\begin{Bmatrix} x \\ y \end{Bmatrix} \tag{6}$$

where m^e_{xx}, c^e_{xx} and k^e_{xx} etc. are all coupling coefficients of single element. And

$$\left.\begin{aligned} m^e_{xx}&=m^e_{yy}=\frac{2\left[1-\left(1-\varepsilon^2\right)^{1/2}\right]}{\varepsilon^2}m^e_a \\ m_{xy}&=m_{yx}=0 \\ c^e_{xx}&=c^e_{yy}=0 \\ c_{xy}&=-c_{yx}=\Omega m^e_a \\ k^e_{xx}&=-\frac{\Omega^2}{4}\frac{1}{\left(1-\varepsilon^2\right)^{1/2}}m^e_a \\ k^e_{yy}&=-\frac{\Omega^2}{4}(1-\varepsilon^2)^{1/2}m^e_a; \\ k^e_{xy}&=k^e_{yx}=0 \\ m^e_a&=\frac{\pi R^2\rho}{\delta}L^e \end{aligned}\right\} \tag{7}$$

with m^e_a denoting the added mass of the fluid flow around the specified element. And L^e is the actual length of the element. ρ is the density of the fluid, here it is 1000kg/m^3.

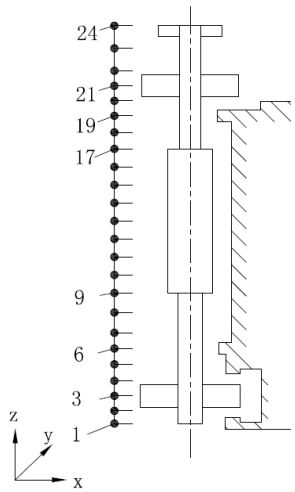

Fig. 2. Finite element model of the RCP.

In Eq. (7), dimensionless parameter ε denotes the initial eccentricity of the rotor, while dimensionless value $\delta=H/R$ representing the ratio of the nominal depth of the fluid annulus H and the rotor radius R. It is of importance to point out that in the present work the value of δ is different from the original work done by Antunes *et al.* [4, 5]. Antunes *et al.* performed the analysis with δ near 0.1 and the present work takes δ near 0.02. However, from [4], they showed that the pressure fields are slightly different in the cases of δ equal 0.1 and 0.01 when ε is

approaching zero. And all the coupling coefficients appear in Eq. (7) are derived with the same ε value. Therefore, despite the difference in the values of δ, the original results in [4] are still applicable in the present analysis as long as ε is zero. In fact, this is the case for RCP stability analysis. Take $\varepsilon = 0$, and work out the limits for some coupling coefficients, there come

$$m_{xx}^e = m_{yy}^e = m_a^e;$$
$$k_{xx}^e = k_{yy}^e = -\frac{\Omega^2}{4} m_a^e; \tag{8}$$

leaving the rest of Eq. (7) unchanged.

From Fig. 2, it is obvious that elements from 9 to 16 are in the annular flow area, where the canned motor of RCP is. In the following numerical computation, only nodes from 10 to 16 have the fluid-structure interaction force applied. And the added coupling coefficient matrices of inertia, damping and stiffness are written in Annex A with the notations of $[M_{fs,x}]$, $[C_{fs,xy}]$, $[K_{fs,x}]$, $[M_{fs,y}]$, $[C_{fs,yx}]$ and $[K_{fs,y}]$. This results in

$$\left[M_{fs}\right] = \begin{bmatrix} M_{fs,x} & \\ & M_{fs,y} \end{bmatrix}; \left[C_{fs}\right] = \begin{bmatrix} & C_{fs,xy} \\ C_{fs,yx} & \end{bmatrix};$$
$$\left[K_{fs}\right] = \begin{bmatrix} K_{fs,x} & \\ & K_{fs,y} \end{bmatrix} \tag{9}$$

where the last two matrices are the functions of angular speed of the rotor, Ω.

Thrust bearing

Normally, thrust bearing is for balancing the axial force of the rotor. Indeed, thrust bearing on RCP can apply a dynamic moment onto the rotor. If all of the aspects of thrust bearing are to be considered, the complicity of the problem will increase significantly. For the absence of axial load of the RCP impeller, the effect of thrust bearing can be modeled as a pair of moments [10]. Like the treatment for the annular flow, the moment on the node of the specified element is

$$\begin{Bmatrix} M_{tb,x}^e \\ M_{tb,y}^e \end{Bmatrix} = -\begin{bmatrix} c_{\varphi\varphi}^{e,M} & c_{\varphi\psi}^{e,M} \\ -c_{\psi\varphi}^{e,M} & -c_{\psi\psi}^{e,M} \end{bmatrix} \begin{Bmatrix} \dot{\varphi} \\ \dot{\psi} \end{Bmatrix}$$
$$-\begin{bmatrix} k_{\varphi\varphi}^{e,M} & k_{\varphi\psi}^{e,M} \\ -k_{\psi\varphi}^{e,M} & -k_{\psi\psi}^{e,M} \end{bmatrix} \begin{Bmatrix} \varphi \\ \psi \end{Bmatrix} \tag{10}$$

where $\varphi=\theta_y$, $\psi=-\theta_x$. It is worth to be note that the inter coupling effect, that is the relation between the translational displacements and the angular deflection, is dropped for simplification. The superscripts, e, can be omitted with the fact that only one node is attached to the thrust bearing in the entire finite element model.

Another two coefficient matrices are shown in Annex B, and they are $[C^M_{tb}]$ and $[K^M_{tb}]$. For the case of RCP, the external moment on the rotor is zero, indicating that left side of Eq. (10) is a zero vector.

Full finite element model

Considering all the factors discussed above, including the basic finite element model of the rotor, the fluid-structure interaction of the annular flow and the moment form the thrust bearing, the full finite element model is

$$\left[M_r + M_{fs}\right]\left\{\ddot{U}\right\} + \left[C_r + C_{fs} + C_{tb}^M\right]\left\{\dot{U}\right\}$$
$$+\left[K_r + K_{fs} + K_{tb}^M\right]\left\{U\right\} = \left\{Q\right\} \tag{11}$$

the coefficient matrices of Eq. (11) are described in Eq. (5) (9) and (10). Equation (11) can turn into

$$\left[M\right]\left\{\ddot{U}\right\} + \left[C\right]\left\{\dot{U}\right\} + \left[K\right]\left\{U\right\} = \left\{Q\right\} \tag{12}$$

where $[M]$, $[C]$ and $[K]$ are self-evident.

STABILITY ANALYSIS OF RCP

Critical speed, modal analysis

One of the characteristics that reveal the essence of RCP rotor dynamics is the critical speed. Let

$$\left\{V\right\} = \begin{Bmatrix} \dot{U} \\ U \end{Bmatrix} \tag{13}$$

to be a state space variable. For the homogeneous form, Eq. (12) can be written as

$$\left[A\right]\left\{\dot{V}\right\} + \left[B\right]\left\{V\right\} = \left\{0\right\} \tag{14}$$

where

$$\left[A\right] = \begin{bmatrix} M & \\ & K \end{bmatrix}, \left[B\right] = \begin{bmatrix} C & K \\ -K & 0 \end{bmatrix} \tag{15}$$

Assume $\{V\}=\{V_0\}e^{vt}$, Eq. (14) turns in to a eigenvalue problem, the imaginary part of every eigenvalue is a whirling speed of RCP.

Figure 3 shows the results when only the annular flow is considered, comparing with the normal case. In Fig. 3, the rotor dynamics of RCP reveals that the value of critical speed will decrease greatly. The homogeneous speed line intersects the first whirling speed (modal speed) line at about 1060rpm while crossing the normal results line at about 1780rpm. The numerical computation also shows that the whirling speeds have much lower value, due to the added mass, than the normal case,

and decrease with a steep trend. When the speed of the rotor of RCP approaches 3050rpm, the first whirling speed will disappear. It comes back when the speed of the rotor passes 3550rpm. In Fig. 3, the line of the first whirling speed makes a jump at the above two speed values because the second becomes the whirling speed with the smallest absolute value. However, the formulation of the added mass used here may need further investigation due to the different dimension of the reduced gap comparing to Antunes *et al.* [4].

The situations with only the thrust bearing are more complicated. The existence of thrust bearing may enhance the stability of RCP, with an example shown in Fig. 4. In Fig. 4, the critical speed increases with a small value and the second and third whirl speeds are also on the figure. This feature thrust bearing brings is useful when the RCP is designed to work under the critical speed, since the margin of safety has been broaden. However, in this simulation, the effect of thrust bearing with different stiffness or damping coefficients will change, and will not guarantee permanent benefit. Figure 5 and Fig. 6 show how the effect of thrust bearing changes when the stiffness and damping coefficients take values in a possible range, respectively. The computation is done in a sense of isotropic bearing which means the stiffness or damping coefficients on diagonal of Eq. (10) have the same absolute value. Besides, in Eq. (10), $k_{\varphi\varphi}$ and $k_{\psi\psi}$ have opposite sign while the other two are zero. And arrange the damping coefficients in the same manner. Figure 5 and Fig. 4 shows that the critical speed of RCP increases when the stiffness of thrust bearing is under 2.0e7 Nm/rad. Figure 6 shows that the rotor bearing system has higher critical speeds when the values of damping coefficients are above 1.0e5 Nms/rad.

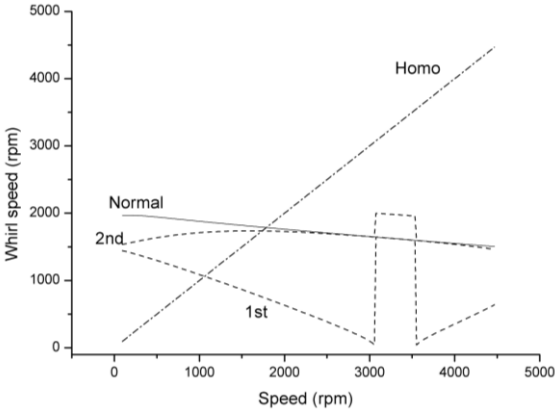

Fig. 3. Critical speed with annular flow.

Stable range analysis

From modal analysis the stability characteristic can be derived from the complex eigenvalues of the system, Eq. (14). The eigenvalues are in the form $\lambda_j=\sigma_j\pm i\nu_j$, where ν_j is the corresponding whirling speed. For an arbitrary eigenvalue λ_j, the relative whirl motion becomes unstable if $\sigma_j>0$. When only consider the whirling speed with the smallest absolute value and in both forward and backward whirl direction, the stability characteristic of the RCP rotor bearing system can be described in Fig. 7-10. The black regions in these figures stand for unstable angular speed (not the value of whirling speed), at which the RCP will give an unstable whirl motion, either forward or backward. The horizontal dashed lines in these figures represent the computation range, from 955 to 4770rpm, of angular speed.

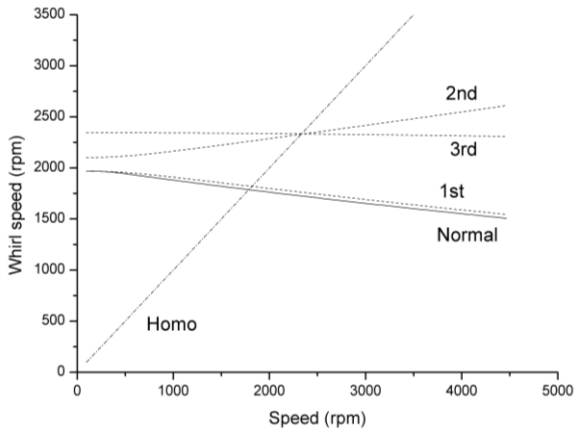

Fig. 4. Critical speed with thrust bearing. Stiffness 1.0e7 Nm/rad; Damping 1.0e6 Nms/rad.

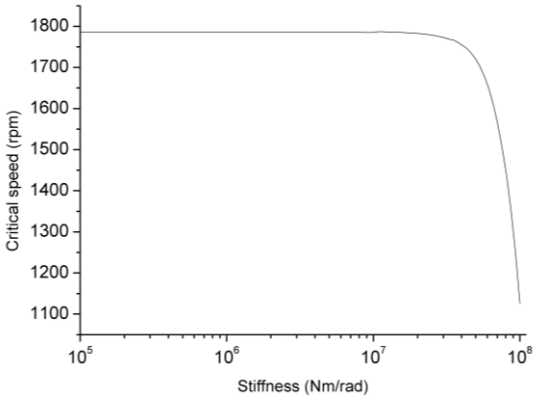

Fig. 5. Critical speed with different stiffness of thrust bearing. Damping 5.0e4 Nms/rad.

Figure 7 and Fig. 8 show the stability feature of RCP with different stiffness of thrust bearing. The RCP will experience stable whirl, both forward and backward, if the angular speed is under 3500rpm. For speed higher than 3500rpm, the backward whirl motion will become unstable in the whole range of concerned stiffness with damping ratio of 1.0e4 Nms/rad. And the forward whirl motion will be unstable only at several operation speed points with the stiffness around 1.0e8 Nm/rad.

However, the cases of damping are slightly irregular. For forward whirl in Fig. 9, it is unstable at some angular speed regions with damping exceeding 5.0e5 Nms/rad. In Fig. 10, it is unstable when the angular speed is higher than 3500rpm, the same result with Fig. 8. And there will be additional unstable

speed range if the damping exceeds 5.3e4 Nms/rad. From Fig. 9 and Fig. 10, both stable forward and backward whirl motions are available as long as the damping of thrust bearing is less than 5.3e4 Nms/rad and operation speed is under 3500rpm.

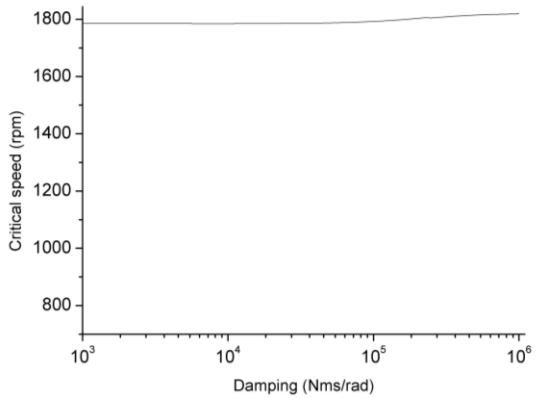

Fig. 6. Critical speed of different damping of thrust bearing. Stiffness 5.0e7 Nm/rad.

Certain agreement exists among these four figures, Fig. 7 to Fig. 10. The stability characteristic in Fig. 8 with damping of 1.0e4 Nms/rad are the same in Fig. 10 with stiffness of 1.0e7 Nm/rad, vice versa. Stable whirl motion can be found between Fig. 7 and Fig 9 within wide range of stiffness and damping coefficients.

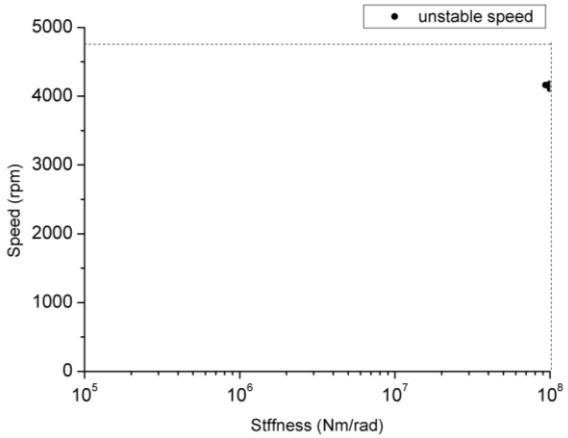

Fig. 7. Stability chart, forward whirl. Damping 1.0e4 Nms/rad.

In the case of thrust bearing having stiffness and damping coefficients of 1.0e7 Nm/rad and 1.0e4 Nms/rad respectively, two detailed figures are given in Fig. 11 and Fig. 12. Like Fig. 3, the first forward whirl disappears at speed of about 3000rpm, and the second forward whirl becomes the first. It comes back at about 3600rpm, but as an unstable backward whirl. In Fig. 12, the damping ratio is calculated from

$$\zeta_j = -\frac{\sigma_j}{\sqrt{\sigma_j^2 + \nu_j^2}} \tag{16}$$

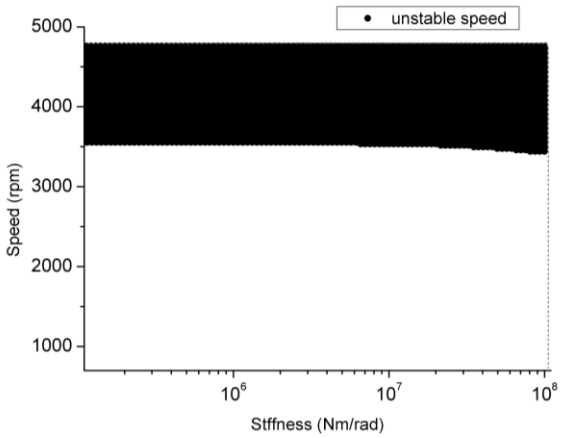

Fig. 8. Stability chart, backward whirl. Damping 1.0e4 Nms/rad.

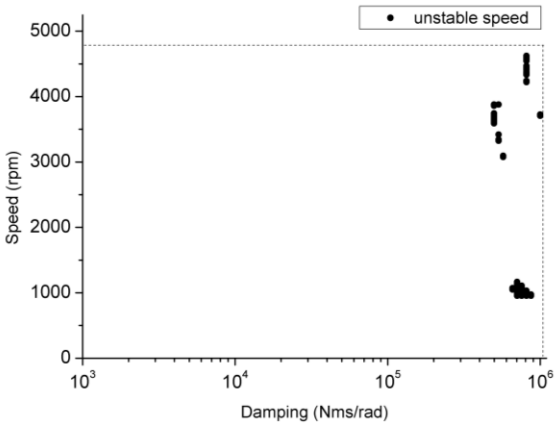

Fig. 9. Stability chart, forward whirl. Stiffness 1.0e7 Nm/rad.

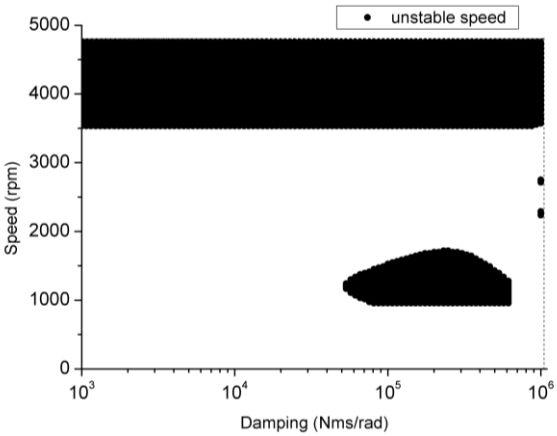

Fig. 10. Stability chart, backward whirl. Stiffness 1.0e7 Nm/rad.

and the value for backward whirl is very small before the speed passes 3500rpm, but still positive denoting a stable state. It becomes negative when the speed is higher than 3500rpm, and

the first backward whirl becomes unstable. On the other hand, the first forward whirl is always stable across the speed range presented, with positive damping ratio. This behavior of whirl motion is consistent with the results shown by Fig. 7 and Fig. 8.

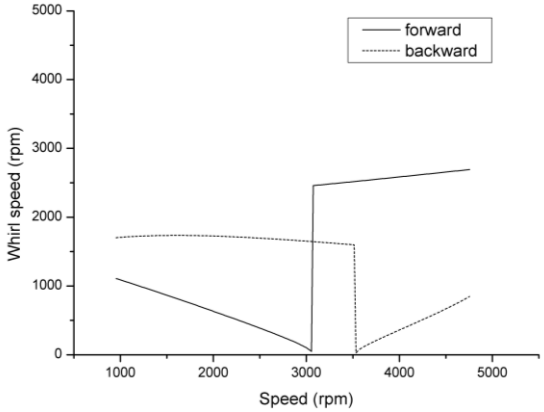

Fig. 11. Whirl speed, results from eigenvalue problem. Stiffness 1.0e7 Nm/rad, damping 1.0e4 Nms/rad.

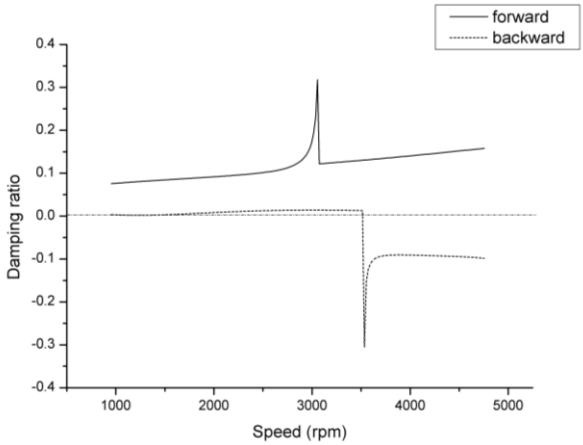

Fig. 12. Damping ratio, results from eigenvalue problem. Stiffness 1.0e7 Nm/rad, damping 1.0e4 Nms/rad.

CONCLUSION

A finite element model for stability analysis of RCP rotor dynamics has been built, in view of the effects from annular flow and the thrust bearing, and numerical computation gives some interesting results. The critical speed of RCP will be lowered because of the added mass, which comes from the fluid in the gap between the rotor and stator of the canned motor, but it needs further investigation. For a wide range of stiffness of thrust bearing, stability is enhanced if the RCP is designed to work at the angular speed under the critical value. On the other hand, the damping level has to be sufficiently high if the same enhancement is expected. For a wide range of stiffness and damping of thrust bearing, stability charts are given with good inter consistence. The stability charts suggest that the RCP rotor bearing system can have both stable forward and backward whirl motions (with speeds of smallest absolute value), at speeds lower than 3500rpm if the value of damping is under 5.3e4 Nms/rad.

ACKNOWLEDGMENTS

This study is supported by China “973” Project (No. 2009CB724300) and China Postdoctoral Science Foundation (No.20110490717).

REFERENCES

[1] Fritz, R., 1970, “The Effects of an Annular Fluid on the Vibrations of a Long Rotor: Part 1-Theory,” ASME Journal of Basic Engineering **92**, pp. 923 – 929.

[2] Ramsden, J., Ritchie, G, and Gupta, J., 1974, “The Vibrational Response Characteristics of a Design for the Sodium Pumps of the Commercial Fast Reactor,” *Proceedings I. Mech. E. Fluid Machinery and Nuclear Energy Groups Convention: Pumps for Nuclear Power Plant*, Bath, April 1974. Paper C107 / 74, pp. 187 – 196.

[3] Ramsden, J., Jones, H. and Cowking, E., 1975 “Vibration of the P.F.R. Primary Sodium Pumps,” *Vibrations and Noise in Pump, Fan and Compressor Installations*. Southampton, September 1975. Paper C103 / 75, pp. 21 – 33.

[4] Antunes, J., Axisa, F., and Grunenwald, T., 1996, “Dynamics of Rotors Immersed in Eccentric Annular Flow. Part 1: Theory,” Journal of Fluids and Structures **10**, pp. 893-918.

[5] Grunenwald, T., Axisa, F., and Bennett, G., 1996, “Dynamics of Rotors Immersed in Eccentric Annular Flow. Part 2: Experiments,” Journal of Fluids and Structures **10**, pp. 919-944.

[6] Moreira, M., Antunes, J., and Pina, H., 2003, “An improved linear model for rotors subject to dissipative annular flows,” Journal of Fluids and Structures **17**, pp. 813-832.

[7] Marscher, W., 1986, “The Effect of Fluid Forces at Various Operation Conditions on the Vibrations of Vertical Pumps,” Radial Loads and Axial Thrusts on Centrifugal Pumps, pp. 17-38.

[8] Mittwollen, N., Hegel, T., and Glienicke, J., 1991, “Effect of hydrodynamic thrust bearings on lateral shaft vibrations.” Transactions ASME Journal of Tribology **113**, pp. 811-818.

[9] Jiang, P.L. and Yu, L., 1999, “Dynamics of A Rotor-Bearing System Equipped with A Hydrodynamic Thrust Bearing,” Journal of Sound and Vibration **227**(4), pp. 833-872.

[10] Jiang, P.L. and Yu, L., 2000, “Identification of the Oil-Film Dynamic Coefficients in a Rotor-Bearing System with a Hydrodynamic Thrust Bearing,” Journal of Sound and Vibration **236**(4), pp. 733-740.

ANNEX A

COEFFICIENT MATRICES OF FLUID STRUCTURE INTERACTION

The matrix of coupling stiffness coefficient $[K_{fs,x}]$ is

$$\left[K_{x,fs}\right]=\begin{bmatrix}
[0]_{16\times16} & & & & & & & & & & & & & & & \\
& 0 & & & & & & & & & & & & & & \\
& & 0 & & & & & & & & & & & & & \\
& & & k_{xx}^{9}+k_{xx}^{10} & & & & & & & & & & & & \\
& & & & 0 & & & & & & & & & & & \\
& & & & & k_{xx}^{10}+k_{xx}^{11} & & & & & & & & & & \\
& & & & & & 0 & & & & & & & & & \\
& & & & & & & \ddots & & & & & & & & \\
& & & & & & & & k_{xx}^{14}+k_{xx}^{15} & & & & & & & \\
& & & & & & & & & 0 & & & & & & \\
& & & & & & & & & & k_{xx}^{15}+k_{xx}^{16} & & & & & \\
& & & & & & & & & & & 0 & & & & \\
& & & & & & & & & & & & 0 & & & \\
& & & & & & & & & & & & & 0 & & \\
& & & & & & & & & & & & & & [0]_{14\times14} &
\end{bmatrix}_{48\times48}$$

$[M_{fs,x}]$, $[C_{fs,xy}]$, $[M_{fs,y}]$, $[C_{fs,yx}]$ and $[K_{fs,y}]$ have the similar pattern.

ANNEX B

MATRIX PATTERN FOR THRUST BEARING

The matrices for thrust bearing, $[C^{M}_{tb}]$ and $[K^{M}_{tb}]$., have the following pattern

$$\left[C_{tb}^{M}\right]=\begin{bmatrix}
0_{(2n-2)\times(2n-2)} & & & & & & \\
& 0 & & & & & \\
& & c_{\varphi\varphi}^{M} & \cdots & \cdots & c_{\varphi\psi}^{M} & \\
& & \vdots & 0_{2N\times2N} & & \vdots & \\
& & \vdots & & 0 & \vdots & \\
& & -c_{\psi\varphi}^{M} & \cdots & \cdots & -c_{\psi\psi}^{M} & \\
& & & & & & 0_{(2(N-n)-2)\times(2(N-n)-2)}
\end{bmatrix}_{4N\times4N}$$

N = 24, n = 5 for this paper.